Available online at www.sciencedirect.com
ScienceDirect
Electrochemistry Communications 10 (2008) 433–437
electrochemistry communications
www.elsevier.com/locate/elecom

Characterization of the anodic growth and dissolution of oxide films on valve metals

Omar E. Linarez Pérez, Valeria C. Fuertes, Manuel A. Pérez, Manuel López Teijelo *

INFIQC – Departamento de Fisicoquímica, Facultad de Ciencias Químicas, Universidad Nacional de Córdoba, Haya de la Torre y Medina Allende, 5000 Córdoba, Argentina

Received 7 December 2007; received in revised form 31 December 2007; accepted 7 January 2008
Available online 12 January 2008

Abstract

Chemical dissolution processes coupled to anodic oxide growth taking place by a "high-field" conduction mechanism, are considered. The equation for the steady-state current density obtained during potentiodynamic polarization measurements is derived and the effect of the oxide dissolution rate on the overall potentiodynamic behaviour by applying repetitive scans with either fixed or increasing anodic switching potentials is discussed. The procedure for obtaining the current dissolution as well as the parameters that characterize the high-field growth is discussed.

Keywords: Oxides growth; Valve metals; Oxides dissolution; High-field growth; Simulation

1. Introduction

Due to the diversity of properties, passive films and their stability play an important role in recent and future research [1]. Stability of oxide films is relevant in a wide range of phenomena, such as the reactivation of passive titanium [2] or the anodizing of aluminium for producing nanoporous films with applications in microelectronics and interconnections for integrated circuits [3], among others. The growth of anodic oxides on "valve" metals has been studied extensively [1,4] and it is well established that oxide films grow irreversibly by a field-assisted migration of ions through the film following the high-field model [1,5].

The open circuit stability of passive titanium oxide films has been investigated by potentiodynamic reformation experiments [6]. Capacitance measurements have been used extensively to characterize the oxide chemical dissolution process in different electrolytic media [7,8]. The capacitive response is interpreted by assigning the changes in C to changes in film thickness (d), although this type of measurement only provides information directly related to thickness when the dissolution takes place as a single process by film thinning. Ellipsometry has been employed by Blackwood et al. [9] to follow the growth and thinning processes of anodic oxide films on titanium. More recently, we have studied the chemical dissolution of WO_3 anodic films by using in situ ellipsometric measurements in order to determine the influence of different phenomena that take place during the overall oxide dissolution [10,11]. Notwithstanding, the use of cyclic voltammetry either with constant or increasing anodic switching potentials is by far much more simple in order to determine the anodic growth and dissolution characteristics of oxide films on metals.

Cyclic polarization measurements have been employed to interpret the growth and dissolution characteristics of aluminium oxide films through simulations [12]. However, for the case of chemical dissolution the equation used to obtain the dependence of the thickness with time (Eq. (6) in Ref. [12]) is in error since the loss of charge (or thickness)

* Corresponding author. Tel.: +54 351 4334169; fax: +54 351 4334188.
E-mail address: mlopez@fcq.unc.edu.ar (M. López Teijelo).

1388-2481/$ - see front matter © 2008 Elsevier B.V. All rights reserved.
doi:10.1016/j.elecom.2008.01.002

should increases with time. More recently, the dissolution rates of Al_2O_3 passive films in neutral solutions containing NaCl were also determined by analysis of the voltammetric anodic curves using the high-field growth mechanism to model oxide film growth and assuming that dissolution rates were independent of the electric potential distribution at the interface [13]. The voltammetric response was computed by an iterative solution and the values of dissolution rates were obtained by fitting the theoretical voltammograms to the experimental curves.

In this paper, we report on the growth and dissolution behaviour of oxide films on valve metals assuming that growth takes place by high-field transport of ions within the oxide film. Equations for the potentiodynamic response are presented and the approach employed for obtaining the oxide dissolution rate is discussed.

2. Theoretical background

Oxide films with low electronic conductivity grow by ion migration and diffusion. When valve metals are anodically polarized, oxide films grow irreversibly by a field-assisted migration of ions through the film following the so-called "high-field" model [4]. Neglecting electron transfer contributions, the current density, j_{ox}, corresponding to the ionic growth current is given by

$$j \approx j_{ox} = A\exp(\beta\varepsilon) \tag{1}$$

where $\varepsilon = (E - E_o)/d$ is the electric field strength and A and β are temperature-dependent parameters characteristic of the oxide [4,5]. The microscopic interpretation of the parameters A and β has been given previously [4].

For the condition of 100% faradaic efficiency for film growth (no oxide dissolution, oxygen evolution or capacitive charging), the film thickness can be calculated as

$$d = d_o + \frac{M}{nF\delta_{ox}}\int_0^t j_{ox}\mathrm{d}t \tag{2}$$

where d_o is the oxide film thickness initially present, δ_{ox} the oxide density, M the oxide molecular weight, n the number of electrons exchanged and F the Faraday constant.

The equations have been solved for potentiostatic, galvanostatic or potentiodynamic conditions [4]. For the potentiodynamic case [4,5], the application of the linear potential sweep establish a steady-state current value, j_{ss}, which is typical for oxide growth on valve metals, given by

$$j_{ss}\ln\left(\frac{j_{ss}}{A}\right) = \left(\frac{nF\delta_{ox}\beta}{M}\right)\upsilon \tag{3}$$

where υ stands for the potential scan rate.

In the presence of either chemical or potential assisted dissolution of the oxide [4], Eq. (2) for thickness has to be modified in order to take into account the loss of charge due to oxide dissolution, $Q(t)$, resulting:

$$d = d_o + \frac{M}{nF\delta_{ox}}\left\{\int_0^t j_{ox}\mathrm{d}t - [Q(t)]\right\} \tag{4}$$

Following the same procedure as described in [4], the following relationship that gives the current/time (or current/potential) dependence, is obtained:

$$\frac{\mathrm{d}y}{\mathrm{d}t} = \frac{1}{t}y\ln(y)\left\{1 - \left[\frac{MA}{nF\delta_{ox}\beta\upsilon}\left(y - \frac{1}{A}\frac{\mathrm{d}Q(t)}{\mathrm{d}t}\right)\ln(y)\right]\right\} \tag{5}$$

where

$$y = \frac{j_{ox}}{A} \tag{6}$$

For the case of chemical dissolution of the oxide (dissolution rate independent of potential), $\mathrm{d}Q(t)/\mathrm{d}t$ is constant and represents the dissolution current density, j_d:

$$\frac{\mathrm{d}Q(t)}{\mathrm{d}t} = j_d \tag{7}$$

The rearranged expression for j_{ss} obtained from Eq. (5), is

$$\ln(j_{ss}) = \ln(A) + \left(\frac{nF\delta_{ox}\beta}{M}\right)\left[\frac{\upsilon}{j_{ss} - j_d}\right] \tag{8}$$

Eq. (8) gives the relationship between j_{ss} and υ for given values of the parameters A, β and j_d, besides the physical properties of the oxide.

Simulations of the j/E potentiodynamic profiles for the oxide growth were performed by integration of the differential equation (Eq. (5)) using the Runge–Kutta (fourth order) algorithm written in FORTRAN, employing the boundary conditions given in Ref. [4], p. 250. The potentiodynamic response was simulated for repetitive potential sweeps either with fixed or increasing anodic switching potential for given value of the parameters d_o, υ, A, β and j_d. In order to obtain the j_d values from the $\ln j_{ss}$ vs. (υ/j_{ss}) plots, data were fitted to Eq. (8) employing non-linear least square routines.

3. Results and discussion

Fig. 1 shows the potentiodynamic j/E response for a bismuth electrode by applying repetitive triangular potential sweeps with fixed (Fig. 1a) and increasingly anodic switching potentials (Fig. 1b). The first anodic scan (Fig. 1a) shows that current increases rapidly and, afterwards, it reaches a steady-state value that remains constant in a broad potential range, which is associated with Bi_2O_3 film growth by the "high-field" mechanism [14]. During the second cycle, the current remains very low and increases slightly at potentials exceeding *ca.* 10 V, due to once a given thickness of oxide has been grown, there is no further appreciable growth until the potential reaches values corresponding to the high field condition. Furthermore, experiments with increase of the anodic switching potential (Fig. 1b) show similar features and the current increase for a given cycle starts at potentials close to that corresponding to the anodic switching potential of the previous cycle. The absence of curve crossing in successive cycles indicates that no

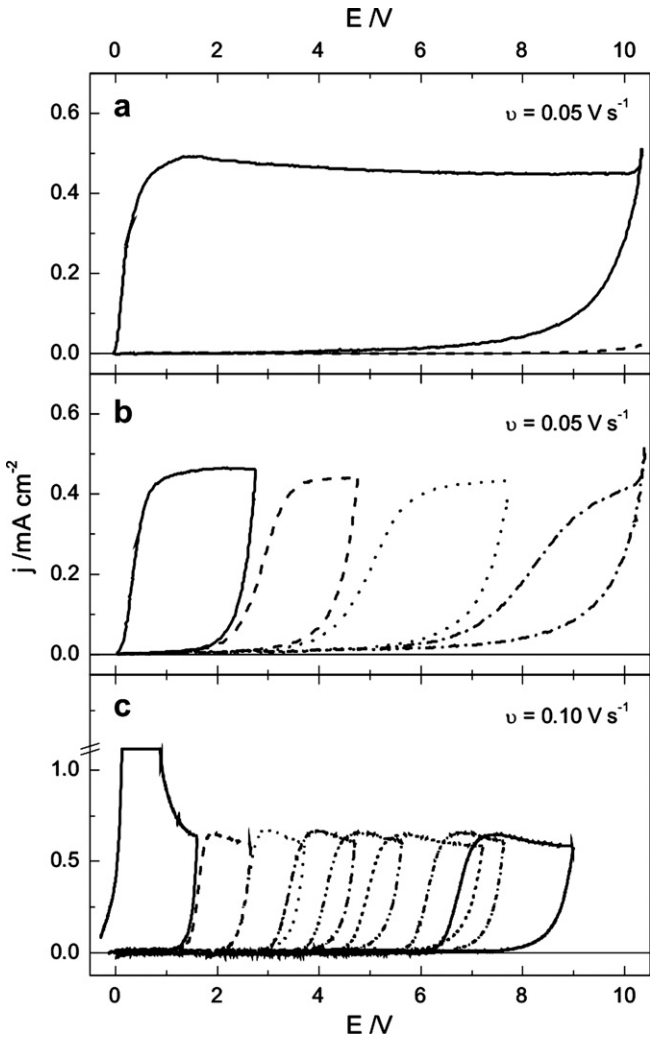

Fig. 1. Potentiodynamic j/E response of bismuth (a, b) in 0.1 M Na_2HPO_4 (pH 10) and tungsten (c) in 1 M $Na_2SO_4 + 0.001$ M H_2SO_4. Repetitive potential sweeps with fixed (a) or increasing (b, c) anodic switching potentials. (—) first and (- - -) second cycles.

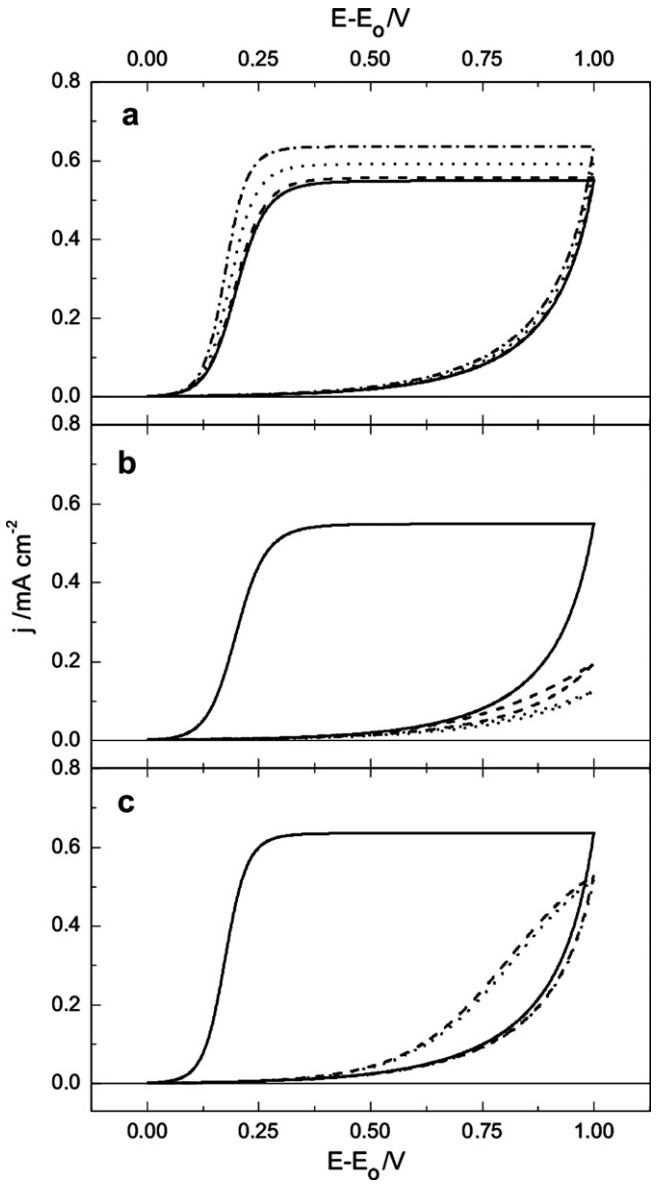

Fig. 2. (a) Simulated potentiodynamic j/E response for the anodic growth of Bi_2O_3 (first cycle) for different chemical dissolution rates (j_d): 0 (—), 10 μA cm^{-2} (- - -), 50 μA cm^{-2} (···), and 100 μA cm^{-2} (-·-·-). (b, c) Simulated potentiodynamic j/E response for the anodic growth of Bi_2O_3 by applying repetitive potential sweeps with fixed anodic switching potential. j_d: 0 (b), and 100 μA cm^{-2} (c). Simulation parameters: $A = 1.3$ μA cm^{-2}, $\beta = 6.0 \times 10^{-6}$ cm V^{-1}, $n = 6$, $M = 465.96$ g mol^{-1}, $\delta = 8.9$ g cm^{-3}, $d_o = 2$ nm, $\upsilon = 0.05$ V s^{-1}. (—) first, (- - -) second, and (···) third cycles.

chemical dissolution of the film is noticeable in the time scale of the experiment. On the contrary, for tungsten (Fig. 1c), it can be seen an important curve crossing between successive cycles due to the increasing importance of chemical dissolution. These features can be employed in order to characterise qualitatively a given system under determined experimental conditions.

Fig. 2a shows the first cycle of the potentiodynamic j/E profiles simulated employing the values of A and β obtained for Bi_2O_3 (see below) at increasing values of the dissolution current, j_d. As j_d increases the current at the initial part of the wave is higher, giving rise to an apparent shifting of the curve towards less positive potentials. The most important change is obtained in the potential region where the steady-state current, j_{ss}, is reached. Once the steady state for growth is established, the value of j_{ss} increases with j_d, although not in a linear fashion as reported in [13]. Figs. 2b, c and 3, show simulated voltammograms for repetitive scans with fixed and increasing anodic switching potentials, respectively. In Fig. 2, it can be seen the current increase in repetitive cycles and the curve shifting towards less negative potentials as j_d increases, while Fig. 3 clearly shows the increasing importance of curve crossing in successive cycles.

Furthermore, the dependence of j_{ss} with υ employing a potentiodynamic perturbation provides the information needed for obtaining the parameters A and β as well as j_d for a given system, as discussed below. In the absence

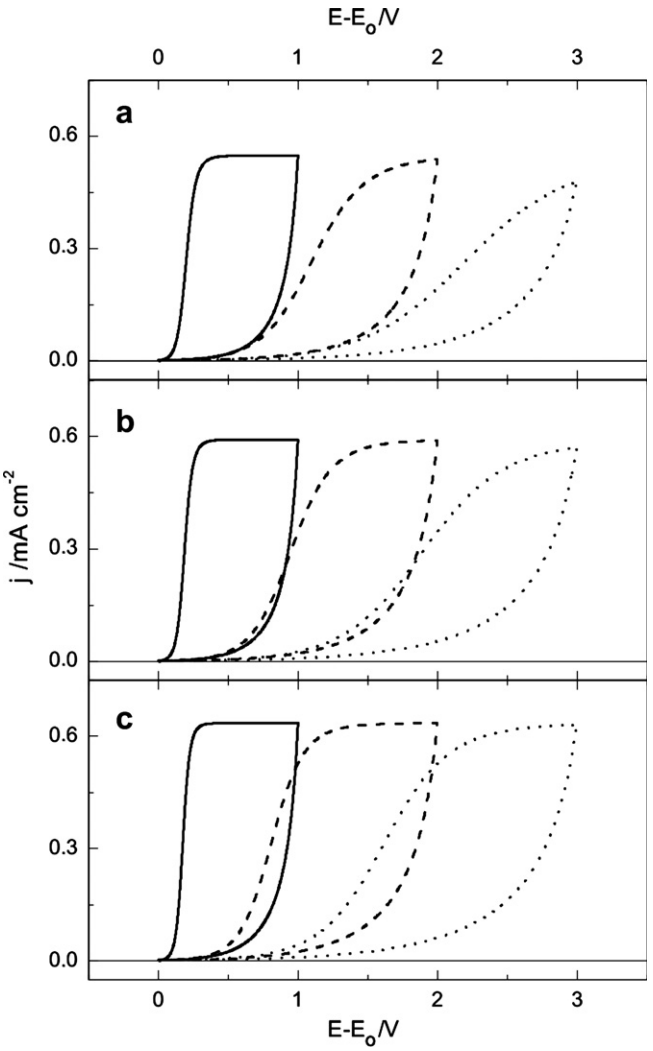

Fig. 3. Simulated potentiodynamic j/E response for the anodic growth of Bi_2O_3 by applying repetitive potential sweeps with increasing switching potential based on the high field conduction model with chemical oxide dissolution. j_d: 0 (a), 50 μA cm^{-2} (b), and 100 μA cm^{-2} (c). Simulation parameters as in Fig. 2.

of chemical dissolution, the usual practice is obtaining the values of A and β from the linear dependence ln (j_{ss}) vs. (υ/j_{ss}) (Eq. (3)) if the physical constants of the oxide are known. On the other hand, in the presence of chemical dissolution Eq. (8) predicts a deviation from linearity as j_d becomes more important in relation to j_{ss}, i.e. at low scan rates. Fig. 4 shows the ln (j_{ss}) vs. (υ/j_{ss}) plot for growth of bismuth oxide in NaOH solutions of different concentration, where chemical dissolution is noticeable. Increasing deviations are seen as C_{OH^-} increases. From the non-linear least square fitting, all the parameters (A, β and j_d) for the different NaOH concentrations were obtained. The values of A and β were constant for the different conditions employed, resulting average values of $A = (1.3 \pm 0.6)$ μA cm^{-2} and $\beta = (6.00 \pm 0.07).10^{-6}$ cm V^{-1}, which are similar to values reported in the literature [1,5,12,15]. Dissolution current increases with C_{OH^-}, as expected (inset in Fig. 4).

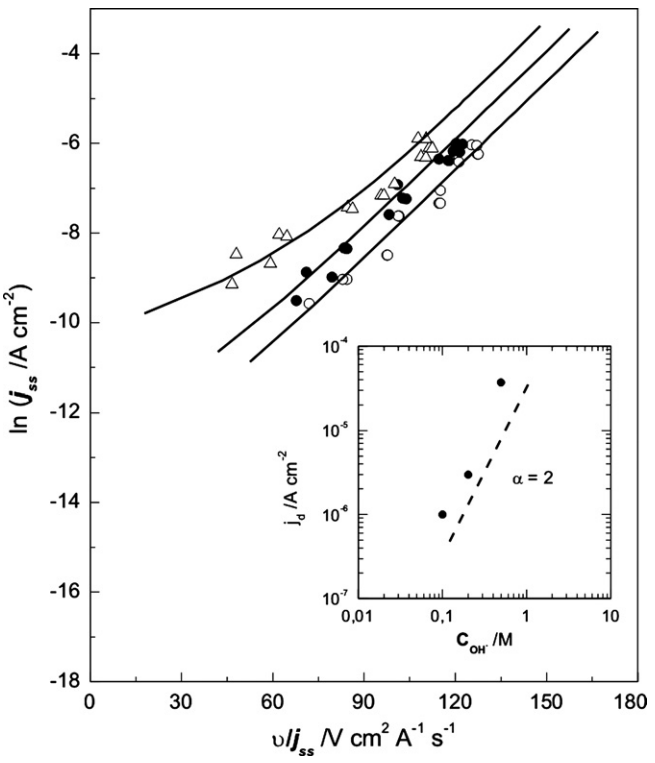

Fig. 4. Plot of ln (j_{ss}) vs. υ/j_{ss} for the anodic growth of Bi_2O_3 in x M NaOH. x: 0.1 (○), 0.2 (●), and 0.5 (Δ). Full lines show the best fit with Eq. (8). Inset: Dependence of j_d values obtained from fitting on C_{OH^-}.

4. Conclusions

Typical voltammograms for oxide growth on bismuth and tungsten are presented in order to show the effect of chemical dissolution coupled to oxide growth. The equation for the steady-state current density obtained in the presence of a chemical dissolution process is derived and the effect of the dissolution rate on the overall potentiodynamic behaviour by applying repetitive scans with either fixed or increasing anodic switching potential is discussed. Based on this equation, the methodology for obtaining the current dissolution as well as the parameters that characterize the high-field growth is presented. The application to the case of potentiodynamic growth and dissolution of bismuth oxide in alkaline solutions allowed obtaining the values of the parameters A and β as well as the current dissolution, j_d.

Acknowledgements

Financial support from CONICET, ANPCYT, ACC S.E. and SECYT-UNC is gratefully acknowledged. OELP acknowledges CONICET for the fellowships granted.

References

[1] J.W. Schultze, M.M. Lohrengel, Electrochim. Acta 45 (2000) 2499.
[2] E.M. Oliveira, C.E.B. Marino, S.R. Biaggio, R.C. Rocha-Filho, Electrochem. Commun. 2 (2000) 254.

[3] A. Mozalev, A. Poznyak, I. Mozaleva, A.W. Hassel, Electrochem. Commun. 3 (2001) 299.
[4] M.J. Dignam, in: J.O'M. Bockris, B.E. Conway, E. Yeager, R.E. White (Eds.), Comprehensive Treatise of Electrochemistry, vol. 4, Plenum Publishing Corporation, 1981 (Chapter 5).
[5] E.M. Patrito, R.M. Torresi, E.P.M. Leiva, V.A. Macagno, J. Electrochem. Soc. 137 (1990) 524.
[6] D.J. Blackwood, L.M. Peter, D.E. Williams, Electrochim. Acta 33 (1988) 1143.
[7] M.M. Hefny, A.G. Gadalla, A.S. Mogoda, B. Electrochem. 3 (1987) 11.
[8] A.S. Mogoda, M.M. Hefny, G.A. El Mahdy, Corros. Sci. 46 (1990) 210.
[9] D.J. Blackwood, R. Greef, L.M. Peter, Electrochim. Acta 34 (1989) 875.
[10] M.A. Pérez, M. López Teijelo, Thin Solid Films 449 (2004) 138.
[11] M.A. Pérez, M. López Teijelo, J. Phys. Chem. B 109 (2005) 19369.
[12] H. Lee, F. Xu, C.S. Jeffcoate, H.S. Isaacs, Electrochem. Solid-State Lett. 4 (2001) B31.
[13] C.J. Boxley, J.J. Watkins, H.S. White, Electrochem. Solid-State Lett. 6 (2003) B38.
[14] M.A. Pérez, O.E. Linarez Pérez, M. López Teijelo, J. Electroanal. Chem. 596 (2006) 149.
[15] O.E. Linarez Pérez, V.C. Fuertes, M.A. Pérez, M. López Teijelo, in: Proceedings of the Symposium on Corrosion, The Electrochemical Society, PV 2001-22, 2001, pp. 99–106.